

EXPRESS LETTER

A probabilistic assessment of sea level variations within the last interglacial stage

Robert E. Kopp,¹ Frederik J. Simons,² Jerry X. Mitrovica,³ Adam C. Maloof² and Michael Oppenheimer^{2,4}

¹Department of Earth and Planetary Sciences and Rutgers Energy Institute, Rutgers University, Piscataway, NJ 08854, USA.

E-mail: robert.kopp@rutgers.edu

²Department of Geosciences, Princeton University, Princeton, NJ 08544, USA

³Department of Earth and Planetary Sciences, Harvard University, Cambridge, MA 02138, USA

⁴Woodrow Wilson School of Public and International Affairs, Princeton University, Princeton, NJ 08544, USA

Accepted 2013 January 24. Received 2013 January 24; in original form 2012 September 18

SUMMARY

The last interglacial stage (LIG; *ca.* 130–115 ka) provides a relatively recent example of a world with both poles characterized by greater-than-Holocene temperatures similar to those expected later in this century under a range of greenhouse gas emission scenarios. Previous analyses inferred that LIG mean global sea level (GSL) peaked 6–9 m higher than today. Here, we extend our earlier work to perform a probabilistic assessment of sea level variability within the LIG highstand. Using the terminology for probability employed in the Intergovernmental Panel on Climate Change assessment reports, we find it extremely likely (95 per cent probability) that the palaeo-sea level record allows resolution of at least two intra-LIG sea level peaks and likely (67 per cent probability) that the magnitude of low-to-high swings exceeded 4 m. Moreover, it is likely that there was a period during the LIG in which GSL rose at a 1000-yr average rate exceeding 3 m kyr⁻¹, but unlikely (33 per cent probability) that the rate exceeded 7 m kyr⁻¹ and extremely unlikely (5 per cent probability) that it exceeded 11 m kyr⁻¹. These rate estimates can provide insight into rates of Greenland and/or Antarctic melt under climate conditions partially analogous to those expected in the 21st century.

Key words: Probability distributions; Sea level change; Geomorphology.

1 INTRODUCTION

The last interglacial stage (LIG; *ca.* 130–115 ka) has attracted considerable interest from climate researchers, as it is the most recent Pleistocene interval during which temperatures at both poles and global mean temperature exceeded their Holocene levels. Ice core data suggest that LIG Greenland temperatures peaked about 5 °C warmer than today (Andersen *et al.* 2004; CAPE-Last Interglacial Project Members 2006; Otto-Bliesner *et al.* 2006) and that Antarctic temperatures were about 3–5 °C warmer than pre-Industrial temperatures (Overpeck *et al.* 2006). Analyses of palaeo-temperature data suggest that global mean temperature was ~1.5 °C warmer than today (Turney & Jones 2010) and that global mean sea surface temperature (SST) was 0.7 ± 0.6 °C warmer than pre-Industrial conditions (and hence about 0.2 ± 0.6 °C warmer than today; NOAA National Climatic Data Center 2011; McKay *et al.* 2011). [It is unclear whether the global mean temperature and global mean SST estimates are consistent. McKay *et al.* (2011) have suggested that the global mean temperature estimate is biased towards terrestrial Northern Hemisphere summer temperatures.] Although the inter-

pretation of the LIG as an analogue for a future warmer climate is complicated by differences in insolation resulting from a more eccentric orbit (van de Berg *et al.* 2011), the LIG provides an accessible natural experiment for assessing the impact of warmer polar temperatures on ice sheet volumes and sea level.

Geological proxies for local palaeo-sea level come from a variety of sources, including corals and coral reef terraces, sedimentary and biological facies, constructional and erosional terraces and hydrological modelling of oxygen isotope records in semi-closed basins. The global marine benthic oxygen isotope record (Lisiecki & Raymo 2005) complements these local sea level records with an entangled joint proxy for benthic temperature and global ice volume. Although, for small changes, mean global sea level (GSL) varies almost linearly with the total loss of land ice, the relationship between land ice mass and local sea level involves complex physical linkages. Notably, the redistribution of mass from land ice to the global ocean alters Earth's gravitational field, topography and rotational state. In the short term, these effects lead to a significant sea level fall near the margins of a melting ice sheet and enhance sea level rise far from the ice sheet by up to ~30 per cent relative to the

global mean (Mitrovica *et al.* 2011); over thousands of years, these effects relax, as solid Earth deformations isostatically compensate for the surface mass (ice plus water) redistribution (Mitrovica & Milne 2003). Superimposed on these ‘static equilibrium sea level’ effects are sea level changes driven by ocean dynamics and temperature and salinity distribution, although these ‘dynamic sea level’ changes are dwarfed by static equilibrium effects resulting from glacial–interglacial swings in ice sheet volume for GSL changes in excess of ~ 20 cm (Kopp *et al.* 2010).

Kopp *et al.* (2009, henceforth K09) used a Bayesian statistical framework that coupled a database of LIG local palaeo-sea level records from 47 localities with the global oxygen isotope record of Lisiecki & Raymo (2005) and a geophysical model of the static equilibrium response of local sea level to ice volume redistribution. We found that LIG GSL peaked considerably higher than today. Using terminology adopted in Intergovernmental Panel on Climate Change (IPCC) assessment reports, we concluded that a rise in LIG GSL ≥ 6.6 m was extremely likely (95 per cent probability), a rise ≥ 8.0 m was likely (67 per cent probability), and that a rise ≥ 9.4 m was unlikely (33 per cent probability). Our result was subsequently confirmed by Dutton & Lambeck (2012) in an independent analysis that employed a different methodology and database but also estimated that LIG GSL peaked between 5.5 and 9 m higher than today.

Local sea level indicators from several sites, including the Bahamas (Chen *et al.* 1991; Hearty *et al.* 2007; Thompson *et al.* 2011), the Yucatán (Blanchon *et al.* 2009), western Australia (Eisenhauer *et al.* 1996), Aldabara Atoll (Braithwaite *et al.* 1973) and the Red Sea (Rohling *et al.* 2008), suggest that sea level was not constant during the LIG but instead underwent one or more falls and advances. The K09 GSL reconstruction showed some evidence of intra-LIG sea level variations, but in that paper we did not investigate the detail of this variation or its robustness. Better understanding of these intra-interglacial sea level variations would be useful for testing hypotheses about, and models of, Greenland and Antarctic ice sheet variability in interglacial conditions, with potential application to future ice sheet changes.

In this paper, we extend the K09 methodology to investigate the robustness and magnitude of intra-LIG sea level variations and provide initial estimates of the associated rates of sea level change.

2 METHODOLOGY

The prior probability distribution for sea level adopted by K09 (Fig. 1) is a multivariate normal empirically derived from 250 alternative land-ice histories, each coupled with one of 72 alternative

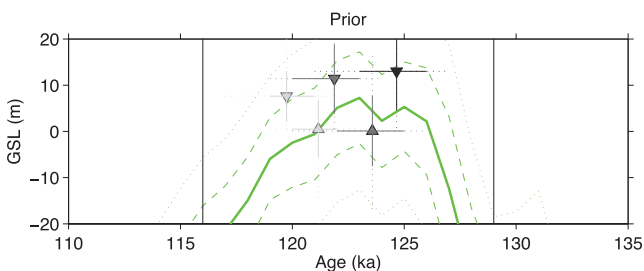


Figure 1. Prior probability distribution for mean global sea level (GSL). Resolved peaks (downward triangles) and troughs (upward triangles) are indicated. Grey tones indicate the probability of existence of peaks (black = 100 per cent, white = 0 per cent). Dashed and dotted error bars represent 67 and 95 per cent confidence intervals, respectively. Because of the broad uncertainty in the prior, the prior expected ages of resolved peaks do not necessarily align with the peaks of the mean of the prior sea level distribution.

solid earth models through a geophysical sea level model. The total land ice volume for each history was sampled from a probability distribution based upon the Lisiecki & Raymo (2005) oxygen isotope stack. The solid earth models are distinguished on the basis of the adopted elastic lithospheric thickness and the viscosities of the upper- and lower-mantle regions. The geophysical modelling is based on a gravitationally self-consistent sea level equation that takes into account viscoelastic deformation of the solid Earth and perturbations to the Earth’s gravitational field and rotational state. The sea level theory takes accurate account of shoreline migration effects (Mitrovica & Milne 2003). To avoid pre-disposing the model to smooth sea level histories, the prior probability distribution allows relatively large swings in sea level, as can be seen by examining the peaks and lows in Fig. 1; we re-examine this assumption later.

Although the age model of our prior distribution for GSL is based upon the Lisiecki & Raymo (2005) timescale, the oxygen isotope curve does not unilaterally dictate the timescale of the posterior probability distribution. As one example of this limited influence, note that, while simple inference from Lisiecki & Raymo (2005) would place GSL at ~ -40 m at 115 ka, the K09 median posterior estimate is -0.5 m.

The K09 sea level database contains 108 distinct LIG sea level observations from 47 sites. Twenty-nine of these observations come from the Red Sea curve of Rohling *et al.* (2008), with a timescale adjusted to align (± 2.5 kyr, 1σ) with that of Lisiecki & Raymo (2005). Although the uncertainties on these observations are relatively large ($\sim \pm 3$ m, 1σ), the Red Sea curve plays an important role in the analysis by anchoring the timescale. The other sites in the database are widely distributed geographically (see fig. 1 of K09).

Let $f(g)$ represent global sea level over time g , \hat{f} the observed sea levels in the database, \hat{t} the measured ages corresponding to these observations and \mathbf{t} the corresponding true ages. After burn-in and thinning (Gilks *et al.* 1995), K09 generated 2500 Markov Chain Monte Carlo (MCMC) samples from $P(\mathbf{t}|\hat{f}, \hat{t})$, the posterior probability distribution of observation ages, conditioned upon the sea level and age observations. Each sample \mathbf{t}_i of \mathbf{t} defines a multivariate normal probability distribution for GSL conditioned upon sea level observations and the sampled ages, with mean $\hat{f}_i(g)$ and covariance Σ_i , such that we can write $P[f(g)|\hat{f}, \mathbf{t}_i] \sim \mathcal{N}[\hat{f}_i(g), \Sigma_i]$. Our notation distinguishes between (1) the measured sea levels \hat{f} and ages \hat{t} , as recorded in the database; (2) a particular set of MCMC samples of true observation ages \mathbf{t}_i ; and (3) the GSL curve over time, conditional upon a particular MCMC sample of observation ages, $P[f(g)|\hat{f}, \mathbf{t}_i]$.

For a particular sample, we consider GSL at a given time point g to be ‘well resolved’ if two criteria are satisfied: (1) $P[f(g)|\hat{f}, \mathbf{t}_i]$ has a posterior standard deviation < 30 per cent of the standard deviation of its prior $P[f(g)]$ and (2) in the analysis employing the full database, the standard deviation of all $\hat{f}_i(g)$ is less than 10 m. The second criterion limits our focus to the time interval 129–116 ka. This definition of ‘well resolved’ is slightly different from that of K09, which employed only the first criterion (see fig. 4 of K09). Moreover, the definition is more conservative, as it excludes an ambiguous pre-129 ka highstand that is highly contingent on the particular sampled values of \mathbf{t}_i and separated from the body of the highstand by a well-resolved interval with $\text{GSL} < -15$ m.

For each sample \mathbf{t}_i , we take 100 values from $P[f(g)|\hat{f}, \mathbf{t}_i]$, considering only those time points g that are well resolved. For a particular value from $P[f(g)|\hat{f}, \mathbf{t}_i]$, we identify the broad LIG highstand as the interval between 140 and 105 ka bounded by intervals during which GSL is greater than or equal to its present level. We identify the peaks and troughs of GSL that are well resolved within this

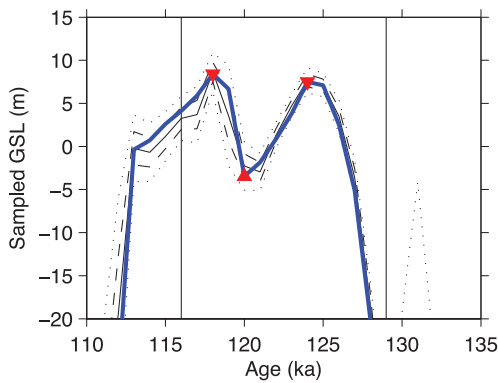


Figure 2. Peak identification example. The black curves show a distribution for GSL conditional upon a particular sample from the probability distribution for observation ages (solid: mean; dashed: 67 per cent confidence interval; dotted: 95 per cent confidence interval). The blue curve shows a single subsample from this distribution. The triangles indicate the identified peaks and lows of this subsample.

interval. Fig. 2 shows one example, in which the highstand extends from 126 to 113 ka, and two peaks and one trough are well resolved.

To test our methodology, we evaluated it using 20 pseudo-proxy data sets, described in the Supporting Information accompanying K09. To generate each data set, a known (randomly generated) sea level history was sampled with pseudo-proxy observations at the same locations and with the same characteristic sea level and age uncertainties as the actual observations in the database. The resulting analysis (Fig. S1) suggests that the methodology presented here performs reasonably well: 57 per cent of the data sets have true maximum rates of intra-LIG sea level change in excess of the projected 50 per cent probability exceedance values; 52 per cent of the data sets have true sea level maxima in excess of the projected 50 per cent probability exceedance values; and 75 per cent of the data sets have true sea level low-to-high swings in excess of the projected 50 per cent probability exceedance values. The analysis does appear to overestimate the uncertainty in its projection of the sea level maxima for the pseudo-proxy data; in all 20 of the data sets, the true sea level maximum falls between the 54 per cent probability and 32 per cent probability exceedance values.

3 RESULTS

3.1 Main analysis

Figs 3a and 4 (red line) and Tables 1–3 summarize some of the main results of our probabilistic assessment. Within the LIG window shown in Fig. 3, two peaks are identified with 98 per cent confidence, a third with 63 per cent confidence, and a fourth with 6 per cent confidence (Table 1). In the age model constructed by our analysis, the best estimates of the ages of the primary and (if they exist) secondary and tertiary peaks are 123–125 ka (quoted at the approximate 95 per cent range), 116–122 and 116–118 ka.

We begin by considering the upper bound on GSL and the rate of GSL rise anywhere in the LIG time window. We find that, within the LIG period, it is extremely likely (95 per cent probability)/likely (67 per cent)/unlikely (33 per cent)/extremely unlikely (5 per cent) that the highest peak GSL well resolved by observations exceeded 6.4/7.7/8.8/10.9 m (Table 2). Moreover, we find that the fastest kyr-average rate of GSL rise into and during the highstand exceeded 5.1/6.9/8.6/11.6 m kyr⁻¹. These inferences differ slightly from our previous analysis (Kopp *et al.* 2009), which found ex-

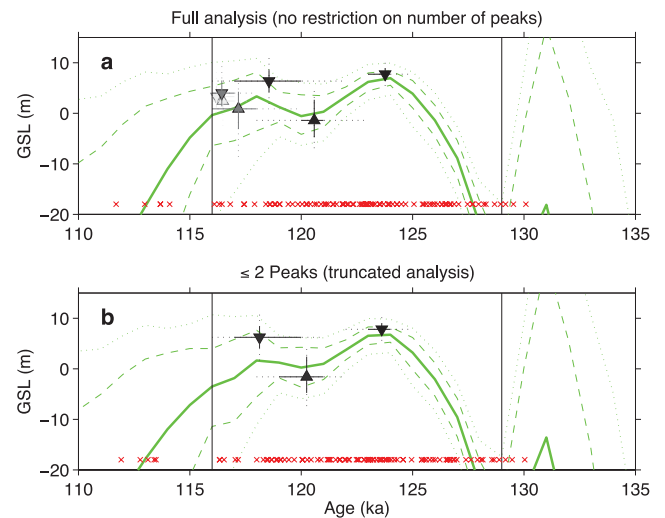


Figure 3. Resolved peaks (downward triangles) and troughs (upward triangles) of the LIG sea level curve. (a) Results of the full analysis. (b) Results with a truncated uniform prior limiting the number of peaks to ≤ 2 . Grey tones indicate the probability of peak existence (black = 100 per cent, white = 0 per cent). Solid, dotted and dashed green lines indicate the mean GSL estimate and its 67 and 95 per cent confidence intervals, respectively. Red crosses show the mean estimates of the ages of sea level observations.

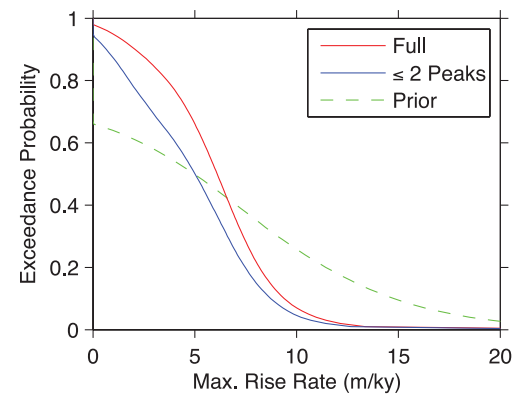


Figure 4. Exceedance probabilities (i.e. the probability the value exceeds a given level) for the maximum rate of sea level rise following the initial GSL peak. The red curve shows the results of the main analysis, while the blue curve shows the results with a truncated uniform prior limiting the number of peaks to ≤ 2 . The dashed green line indicates the prior.

tremely likely/likely/unlikely exceedance values of 6.6/8.0/9.4 m and 5.6/7.4/9.2 m kyr⁻¹, because we limit our focus to the post-129 ka highstand clearly resolved by the data. That is to say, the current analysis excludes a possible ~ 132 ka peak whose resolution depends upon the interpretation of geochronological uncertainties and is separated from the main body of the LIG by a well-resolved interval of GSL < -15 m; see Fig. 3.

Considering only changes following the initial sea level peak, we find that the sea level low-to-high swing exceeded 1.1/7.8/11.2/15.1 m (Table 3), and that the maximum kyr-average rate of GSL rise within the LIG exceeded 1.0/4.9/7.2/10.6 m kyr⁻¹ (Table 4).

3.2 Truncated analysis

The K09 prior probability distribution did not explicitly constrain the number of sea level peaks during the last interglacial, as we

Table 1. Probability of global sea level peak identification.

Number of peaks	1	2	3	4	5
Full MCMC analysis	100 %	98 %	63 %	6 %	0 %
≤2 Peaks	100 %	95 %	0 %	0 %	0 %
No Red Sea (MCMC)	100 %	100 %	97 %	70 %	19 %
No Red Sea	100 %	100 %	85 %	40 %	7 %
Only Red Sea	100 %	51 %	3 %	0 %	0 %
Only Best+RS	100 %	98 %	56 %	5 %	0 %
Only Best−RS	100 %	100 %	79 %	29 %	3 %
Prior	97 %	66 %	17 %	1 %	0 %

Table 2. Maximum global sea level peak height (m).

Exceedance probability	95th	67th	50th	33rd	5th
Full MCMC analysis	6.4	7.7	8.2	8.8	10.9
≤2 Peaks	6.3	7.6	8.1	8.7	10.8
No Red Sea (MCMC)	6.8	8.5	9.3	10.2	14.0
No Red Sea	6.4	7.8	8.4	9.1	11.9
Only Red Sea	3.5	5.2	5.9	6.6	8.5
Only Best+RS	5.9	7.3	7.9	8.6	11.2
Only Best−RS	6.0	7.6	8.3	9.1	11.9
Prior	2.0	11.1	14.6	18.3	29.0

did not wish to be prescriptive in this regard. As a consequence, mismatched age models between different observations could lead to an overestimate of the number of peaks. One might therefore reasonably hold an implicit prior that judges fewer peaks to be more likely than more peaks. The absence of any known site with geomorphological indicators recording more than two sea level peaks supports this implicit prior. In the absence of a particular form for this prior, we conduct a sensitivity analysis employing a truncated uniform distribution for the number of peaks; that is, we consider only the 37 per cent of cases in which the models find ≤2 LIG sea level peaks (Fig. 3 b and Fig. 4, blue line.)

Table 3. Maximum intra-LIG GSL low-to-high swing (m).

Exceedance probability	95th	67th	50th	33rd	5th
Full MCMC analysis	1.1	7.8	9.6	11.2	15.1
≤2 Peaks	0.0	4.4	8.2	10.2	14.5
No Red Sea (MCMC)	3.8	6.1	7.1	8.2	12.0
No Red Sea	3.0	7.0	8.5	10.1	15.5
Only Red Sea	0.0	0.0	0.1	2.7	8.5
Only Best+RS	0.8	8.4	10.3	11.8	15.6
Only Best−RS	2.0	5.9	7.3	9.0	14.1
Prior	0.0	0.0	6.1	10.9	23.9

Table 4. Maximum intra-LIG global sea level rise rate (m kyr^{−1}).

Exceedance probability	95th	67th	50th	33rd	5th
Full MCMC analysis	1.0	4.9	6.1	7.2	10.6
≤2 Peaks	0.0	3.3	5.0	6.4	9.9
No Red Sea (MCMC)	2.6	4.4	5.2	6.1	9.5
No Red Sea	2.1	4.8	5.8	6.9	10.9
Only Red Sea	0.0	0.0	0.1	2.3	7.2
Only Best+RS	0.8	5.2	6.5	7.6	10.8
Only Best−RS	1.3	3.8	5.0	6.2	10.2
Prior	0.0	0.0	5.0	8.5	17.6

The truncation has almost no effect on our estimate of peak sea level, which under the truncated prior exceeded 6.3/7.6/8.7/10.8 m (~10 cm less than in the untruncated analysis; Table 2). It does somewhat reduce the maximum rate of rise into and during the LIG, which in this analysis exceeded 4.9/6.6/8.2/11.2 m kyr^{−1} (0.3–0.4 m kyr^{−1} slower). A second sea level peak during the LIG is resolved with 95 per cent confidence (Table 1). Considering only changes following the initial sea level peak, the sea level low-to-high swing exceeded 0.0/4.4/10.2/14.5 m (Table 3); the maximum kyr-average rate of GSL rise within the LIG exceeded 0.0/3.3/6.4/9.9 m kyr^{−1} (Table 4).

3.3 Subset analyses

To assess the contribution of different data to our results, we conduct a number of analyses employing subsets of the full database. K09 conducted comprehensive subset analyses, in which the entire MCMC analysis, including consideration of geochronological uncertainties, was run upon limited data sets (see the Supporting Information and fig. S8 of K09). We consider one such subset, the K09 ‘no isotopes’ subset, which excludes the Red Sea curve from the analysis. Here, we refer to this subset as the ‘No Red Sea (MCMC)’ subset. We also consider a number of additional subsets, for which (for reasons of computational economy) we have not rerun the entire MCMC analysis but have instead retained the probability distributions for t_i from the main analysis while using only the subset for the Gaussian process estimation of $P[f(g)|\mathcal{S}, t]$. These subsets are:

- (i) No Red Sea: all except the Rohling *et al.* (2008) Red Sea curve.
- (ii) Only Red Sea: only the Red Sea curve.
- (iii) Only Best+RS: only Bahamas (Chen *et al.* 1991; Hearty *et al.* 2007), Bermuda (Muhs *et al.* 2002; Hearty *et al.* 2007), Western Australia (Murray-Wallace & Belperio 1991; Zhu *et al.* 1993; Stirling *et al.* 1995; Eisenhauer *et al.* 1996; Stirling *et al.* 1998; Hearty *et al.* 2007), Seychelles (Israelson & Wohlfarth 1999), Barbados (Schellmann & Radtke 2004), Oahu (Muhs *et al.* 2002; Hearty *et al.* 2007) and the Red Sea curve.
- (iv) Only Best−RS: as above, but excluding the Red Sea curve.

The sites in the ‘Only Best’ subsets are selected from the database to maximize overlap with the sites considered by Dutton & Lambeck (2012).

Results of the subset analyses are shown in Tables 1–4 and Fig. S2. The Only Red Sea subset less clearly resolves multiple peaks (51 per cent probability of a second peak) (Table 1), has a lower overall maximum height (exceeding 3.5/5.2/6.6/8.5 m; Table 2) and has a lower maximum rate of intra-LIG sea level variations (exceeding 0.0/2.3/7.2 m kyr^{−1}; Table 4). Variations among the other subsets are relatively modest, with the notable exception that all the subsets excluding the Red Sea data have longer high stands and a greater likely number of peaks. With the exceptions of the Only Red Sea and No Red Sea (MCMC) subsets, all subsets yield maximum LIG GSL heights exceeding 5.9–6.4/7.3–7.8/8.6–9.1/10.8–11.9 m (Table 2). The No Red Sea (MCMC) subset yields higher exceedance values, and the Only Red Sea subset lower values. With the exception of the Only Red Sea subset, all yield a ≥95 per cent probability of at least two peaks (Table 1), and a maximum intra-LIG rate of sea level rise likely exceeding 3.8–5.2 m kyr^{−1}, unlikely exceeding 6.1–7.6 m kyr^{−1}, and extremely unlikely exceeding 9.5–10.9 m kyr^{−1} (Table 4).

4 DISCUSSION AND CONCLUSIONS

K09 estimated with 95 per cent confidence that the peak kyr-averaged rate of GSL rise when GSL exceeded -10 m was greater than 5.6 m kyr⁻¹, but that this rate was unlikely (33 per cent probability) to have exceeded 9.2 m kyr⁻¹. They cautioned that kyr-averaged rates could not be used to place an upper bound on the fastest rate of sea level rise over shorter timescales. Moreover, as a few m equivalent eustatic sea level of ice in the Laurentide and/or Eurasian ice sheets likely remained on the planet when $\text{GSL} > -10$ m, these rates may have been dominated by ice loss from one of these ice sheets rather than from a currently extant ice sheet.

Focusing more specifically on intra-LIG sea level observations, if they can be resolved, provides more direct information about the behaviour of the Greenland and Antarctic ice sheets during this period. Since the exceedance probabilities from the ≤ 2 peaks analysis are always less than or equal to those from the untruncated 'full' analysis, we conservatively employ lower bounds from the former and upper bounds from the latter. We therefore conclude that it is extremely likely that our analysis resolves the existence of at least one sizable intra-LIG sea level fall and rise, likely one in excess of 4 m. Moreover, the sea level rise following the lowstand occurred at a maximum kyr-averaged rate that likely exceeded 3 m kyr⁻¹, but was unlikely to have exceeded 7 m kyr⁻¹ and extremely unlikely (5 per cent probability) to have exceeded 11 m kyr⁻¹.

Both the rate and magnitude of the low-to-high GSL swing projected from this analysis are similar to those estimated for local changes in the Bahamas by Thompson *et al.* (2011), whose observations post-dated the compilation of the K09 database and were therefore not included in our analysis. Thompson *et al.* (2011) estimated that an initial peak of 4 m was followed by a low of ≤ 0 m and a high of 6 m, and that the minimum rate of change during this interval was 2.6 m kyr⁻¹. The rates of rise estimated from our analysis are lower than the maximum century-average rates of sea level change at the Red Sea estimated by Rohling *et al.* (2008) (1.6 ± 0.8 m century⁻¹), but given both the difference in timescale (century- versus millennial-average) and geographic scope (global versus Red Sea), the results are not necessarily inconsistent.

While kyr-averaged rates cannot provide an upper bound on shorter-term rates, they can provide a lower bound. Satellite altimetry data indicate that, over the last twenty years, global mean sea surface height has risen by 3.1 ± 0.4 mm yr⁻¹ (Nerem *et al.* 2010); it is therefore likely that sub-millennial intervals of faster GSL rise occurred during the LIG.

Our analysis is limited by geochronological ambiguity among the timescales employed by last interglacial sea level researchers, which amounts to a ~ 2 kyr disagreement on the timing of the LIG highstand between age models based upon open-system U/Th dates and those based upon closed-system U/Th dates (e.g. Thompson *et al.* 2011; Dutton & Lambeck 2012). The K09 analysis, extended here, applied a prior probability distribution based upon the Lisiecki & Raymo (2005) age model. Ongoing work is investigating the consequences of different prior age models, which could alter some of the rates presented here. The truncated ' ≤ 2 peaks' case allows some examination of the effects of geochronological ambiguity on rate estimates, since this truncation selects for samples from the probability distribution with observation ages that maximize coherence rather than increase the number of sea level peaks. This truncation has a modest effect on estimates of rates of change, but does reduce estimates of the magnitude of intra-LIG sea level swings.

The last interglacial is an imperfect analogue for the 21st century. Under most scenarios, LIG-like polar temperatures will likely be achieved by the middle of the century and exceeded by the end of it. On the other hand, Earth's greater eccentricity during the last interglacial led to more intense summer insolation in the Northern Hemisphere and more protracted summer melt periods in the Southern Hemisphere (Huybers & Denton 2008). Van de Berg *et al.* (2011) suggest that insolation changes were responsible for ~ 45 per cent of LIG Greenland melting. Thus it cannot be concluded that LIG-like polar temperatures alone would be sufficient to cause LIG-like ice sheet melt.

The cryosphere is a complex system with inherent stochasticity, and it is unclear to what extent identical climatic forcings would generate identical ice sheet responses. While the ~ 130 m GSL change between glacial low stands and interglacial high stands is deterministically related to climate, the few metres of difference between interglacials may or may not be. Reconstruction of globally integrated records akin to those of the LIG for earlier interglacials can help resolve this question. Leveraging the distinct spatio-temporal presentation of sea level patterns associated with different meltwater sources to reconstruct not just GSL but also changes in individual ice sheets should yield further insight. Despite these caveats, the record of LIG sea level variations suggests that the ice sheets currently extant are likely capable of sustaining rates of melting faster than those observed today for at least a millennium.

ACKNOWLEDGMENTS

We thank the members of the PALSEA (Palaeo-Constraints on Sea Level Rise) working group funded by Past Global Changes/IMAGES (International Marine Past Global Change Study) for helpful discussion. This research was supported by National Science Foundation grant ARC-1203415 to REK. FJS was supported by National Science Foundation grant EAR-1150145.

REFERENCES

- Andersen, K.K. *et al.*, 2004. High-resolution record of Northern Hemisphere climate extending into the last interglacial period, *Nature*, **431**, 147–151.
- Blanchon, P., Eisenhauer, A., Fietzke, J. & Liebetrau, V., 2009. Rapid sea-level rise and reef back-stepping at the close of the last interglacial highstand, *Nature*, **458**, 881–884.
- Braithwaite, C.J.R., Taylor, J.D. & Kennedy, W.J., 1973. The evolution of an atoll: the depositional and erosional history of Aldabra, *Phil. Trans. R. Soc. B*, **266**, 307–340.
- CAPE-Last Interglacial Project Members, 2006. Last Interglacial Arctic warmth confirms polar amplification of climate change, *Quat. Sci. Rev.*, **25**, 1383–1400.
- Chen, J.H., Curran, H.A., White, B. & Wasserburg, G.J., 1991. Precise chronology of the last interglacial period: ²³⁴U-²³⁰Th data from fossil coral reefs in the Bahamas, *Geol. Soc. Am. Bull.*, **103**, 82–97.
- Dutton, A. & Lambeck, K., 2012. Ice volume and sea level during the last interglacial, *Science*, **337**, 216–219.
- Eisenhauer, A., Zhu, Z.R., Collins, L.B., Wyrwoll, K.H. & Eichstatter, R., 1996. The Last Interglacial sea level change: new evidence from the Abrolhos islands, West Australia, *Geol. Rund.*, **85**, 606–614.
- Gilks, W.R., Richardson, S. & Spiegelhalter, D., 1995. *Markov Chain Monte Carlo in Practice: Interdisciplinary Statistics*, CRC Press, Boca raton, FL, USA.
- Hearty, P.J., Hollin, J.T., Neumann, A.C., O'Leary, M.J. & McCulloch, M., 2007. Global sea-level fluctuations during the Last Interglaciation (MIS 5e), *Quat. Sci. Rev.*, **26**, 2090–2112.
- Huybers, P. & Denton, G., 2008. Antarctic temperature at orbital timescales controlled by local summer duration, *Nat. Geosci.*, **1**, 787–792.

- Israelson, C. & Wohlfarth, B., 1999. Timing of the Last-Interglacial high sea level on the Seychelles Islands, Indian Ocean, *Quat. Res.*, **51**, 306–316.
- Kopp, R.E., Simons, F.J., Mitrovica, J.X., Maloof, A.C. & Oppenheimer, M., 2009. Probabilistic assessment of sea level during the last interglacial stage, *Nature*, **462**, 863–867.
- Kopp, R.E., Mitrovica, J.X., Griffies, S.M., Yin, J., Hay, C.C. & Stouffer, R.J., 2010. The impact of Greenland melt on local sea levels: a partially coupled analysis of dynamic and static equilibrium effects in idealized water-hosing experiments, *Clim. Change*, **103**, 619–625.
- Lisiecki, L.E. & Raymo, M.E., 2005. A Pliocene-Pleistocene stack of 57 globally distributed benthic $\delta^{18}\text{O}$ records, *Paleocean.*, **20**, PA1003, doi:10.1029/2004PA001071.
- McKay, N.P., Overpeck, J.T. & Otto-Bliesner, B.L., 2011. The role of ocean thermal expansion in Last Interglacial sea level rise, *Geophys. Res. Lett.*, **38**, L14605, doi:10.1029/2011GL048280.
- Mitrovica, J.X. & Milne, G.A., 2003. On post-glacial sea level: I. General theory, *Geophys. J. Int.*, **154**, 253–267.
- Mitrovica, J.X., Gomez, N., Morrow, E., Hay, C., Latychev, K. & Tamisiea, M.E., 2011. On the robustness of predictions of sea level fingerprints, *Geophys. J. Int.*, **187**, 729–742.
- Muhs, D.R., Simmons, K.R. & Steinke, B., 2002. Timing and warmth of the Last Interglacial period: new U-series evidence from Hawaii and Bermuda and a new fossil compilation for North America, *Quat. Sci. Rev.*, **21**, 1355–1383.
- Murray-Wallace, C. & Belperio, A.P., 1991. The Last Interglacial shoreline in Australia – a review, *Quat. Sci. Rev.*, **10**, 441–461.
- Nerem, R.S., Chambers, D.P., Choe, C. & Mitchum, G.T., 2010. Estimating mean sea level change from the TOPEX and Jason altimeter missions, *Mar. Geod.*, **33**, 435–446.
- NOAA National Climatic Data Center, 2011. *State of the climate: global analysis for annual 2011*, published online Dec. 2011, Last accessed 24 January 2012. <http://www.ncdc.noaa.gov/sotc/global/2011/13>.
- Otto-Bliesner, B.L., Marshall, S.J., Overpeck, J.T., Miller, G.H. & Hu, A., 2006. Simulating Arctic climate warmth and icefield retreat in the Last Interglaciation, *Science*, **311**, 1751–1753.
- Overpeck, J.T., Otto-Bliesner, B.L., Miller, G.H., Muhs, D.R., Alley, R.B. & Kiehl, J.T., 2006. Paleoclimatic evidence for future ice-sheet instability and rapid sea-level rise, *Science*, **311**, 1747–1750.
- Rohling, E.J., Grant, K., Hemleben, C.H., Siddall, M., Hoogakker, B.A.A., Bolshaw, M. & Kucera, M., 2008. High rates of sea-level rise during the last interglacial period, *Nat. Geosci.*, **1**, 38–42.
- Schellmann, G. & Radtke, U., 2004. A revised morpho- and chronostratigraphy of the Late and Middle Pleistocene coral reef terraces on Southern Barbados (West Indies), *Earth-Sci. Rev.*, **64**, 157–187.
- Stirling, C.H., Esat, T.M., McCulloch, M.T. & Lambeck, K., 1995. High-precision U-series dating of corals from Western Australia and implications for the timing and duration of the Last Interglacial, *Earth Planet. Sci. Lett.*, **135**, 115–130.
- Stirling, C.H., Esat, T.M., Lambeck, K. & McCulloch, M.T., 1998. Timing and duration of the Last Interglacial: evidence for a restricted interval of widespread coral reef growth, *Earth planet. Sci. Lett.*, **160**, 745–762.
- Thompson, W.G., Curran, H.A., Wilson, M.A. & White, B., 2011. Sea-level oscillations during the last interglacial highstand recorded by Bahamas corals, *Nat. Geosci.*, **4**, 684–687.
- Turney, C. S.M. & Jones, R.T., 2010. Does the Agulhas Current amplify global temperatures during super-interglacials?, *J. Quat. Sci.*, **25**, 839–843.
- van de Berg, W.J., van den Broeke, M., Ettema, J., van Meijgaard, E. & Kaspar, F., 2011. Significant contribution of insolation to Eemian melting of the Greenland ice sheet, *Nat. Geosci.*, **4**, 679–683.
- Zhu, Z.R., Wyrwoll, K.H., Collins, L.B., Chen, J.H., Wasserburg, G.J. & Eisenhauer, A., 1993. High-precision U-series dating of Last Interglacial events by mass spectrometry: Houtman Abrolhos Islands, western Australia, *Earth Planet. Sci. Lett.*, **118**, 281–293.

SUPPORTING INFORMATION

Additional Supporting Information may be found in the online version of this article:

Figure S1. Pseudo-proxy analyses.

Figure S2. Resolved peaks and troughs of the LIG sea level curve for subset analyses (<http://gji.oxfordjournals.org/lookup/suppl/doi:10.1093/gji/ggt029/-/DC1>).

Please note: Oxford University Press is not responsible for the content or functionality of any supporting materials supplied by the authors. Any queries (other than missing material) should be directed to the corresponding author for the article.